



1 Global source apportionment of aerosols into major emission regions
2 and sectors over 1850–2017

3

4

5 Yang Yang^{1*}, Shaoxuan Mou¹, Hailong Wang², Pinya Wang¹, Baojie Li¹, Hong Liao¹

6

7

8

9 ¹Joint International Research Laboratory of Climate and Environment Change (ILCEC),

10 Jiangsu Key Laboratory of Atmospheric Environment Monitoring and Pollution Control,

11 Jiangsu Collaborative Innovation Center of Atmospheric Environment and Equipment

12 Technology, School of Environmental Science and Engineering, Nanjing University of

13 Information Science and Technology, Nanjing, Jiangsu, China

14 ²Atmospheric, Climate, and Earth Sciences Division, Pacific Northwest National Laboratory,

15 Richland, Washington, USA

16

17

18

19

20

21 *Correspondence to yang.yang@nuist.edu.cn



22 **Abstract**

23 Anthropogenic emissions of aerosols and precursor gases have been changing significantly in
24 the past few decades across the world. In this study, an explicit aerosol source tagging system
25 (EAST) is merged into the Energy Exascale Earth System Model version 1 (E3SMv1) to
26 quantify the variations in anthropogenic aerosol concentrations, source contributions, and
27 their subsequent radiative impact in four major emission regions on the globe during 1850–
28 1980, 1980–2010 and 2010–2017. In North America and Europe, changes in anthropogenic
29 $PM_{2.5}$ were mainly caused by changes in emissions from local energy and industrial sectors.
30 The local industrial sector caused the most increase in $PM_{2.5}$ in East Asia during 1980–2010
31 and decrease during 2010–2017. In South Asia, the increase in energy-related emissions
32 dominated the rise of $PM_{2.5}$ levels during 1980–2017. During 1850–1980, the increases in
33 emissions from North America contributed to the increase in European $PM_{2.5}$ burden by 1.7
34 $mg\ m^{-2}$ and the sources from the Europe were also responsible for the $PM_{2.5}$ burden increase
35 in East Asia and South Asia by about 1.0 $mg\ m^{-2}$. During 1980–2010, East Asia contributed
36 to an increase of 0.4–0.6 $mg\ m^{-2}$ in $PM_{2.5}$ burden in North America and Europe, while South
37 Asian contributed about 0.3 $mg\ m^{-2}$. During 2010–2017, the contributions from East Asia to
38 the $PM_{2.5}$ burdens in the North America, Europe and South Asia declined by 0.3–0.6 $mg\ m^{-2}$
39 due to Clean Air actions in China, while the contributions from South Asia still increased due
40 to the continuous increase in emissions in South Asia. The historical changes in aerosols had
41 an impact on effective radiative forcing through aerosol-radiation interactions (ERF_{ari}).
42 During 1980–2010, a decline in North American aerosols resulted in a positive ERF_{ari} change
43 (warming effect) in Europe and a decline of aerosols in Europe caused a warming effect in



44 Russia and northern China. The changes in ERF_{ari} from the increase and decrease of aerosols
45 in China during 1980–2010 and 2010–2017, respectively, are comparable in magnitude. The
46 continuous aerosol increases in South Asia from 1980 to 2017 resulted in negative ERF_{ari}
47 (cooling) changes in South Asia, Southeast Asia, and southern China.



48 **1. Introduction**

49 Atmospheric aerosols, also known as particulate matter (PM), have significant influences
50 on air quality and human health (Anenberg et al., 2010; Finlayson-Pitts and Pitts, 1997; Li et
51 al., 2017; Pöschl, 2005). Aerosols also affect the energy budget of the earth system by
52 scattering and/or absorbing solar radiation, thus directly affecting the climate (Gao et al., 2022;
53 Yang et al., 2020a). Meanwhile, they may act as cloud condensation nuclei and/or ice nuclei,
54 changing cloud characteristics and atmospheric water cycle, which indirectly affect the climate
55 (Liao et al., 2015; Lohmann and Feichter, 2005; Rosenfeld et al., 2008; Yang et al., 2022). Due
56 to the absorption of solar radiation, aerosol-induced heating can strengthen temperature
57 inversion and increase the atmospheric stability, which inhibits the vertical mixing and
58 transport of aerosols and leads to a further increase in near-surface aerosol concentrations
59 (Chen et al., 2021; Lou et al., 2019). Therefore, knowing the sources of aerosols and their
60 variations have become a vital direction in the field of environmental and atmospheric sciences.

61 Human activities have a great influence on global aerosol distributions and compositions.
62 For example, many countries have taken various air quality control measures at different stages
63 of their economic development, causing distinct historical temporal changes of aerosol
64 emissions across the world. Since the start of industrialization, anthropogenic emissions of
65 aerosols and precursor gases have substantially increased, which significantly affected the
66 atmospheric environment and the Earth's energy balance (Carslaw et al., 2013). European and
67 North American countries became major contributors of pollutant emissions. Since the 1980s,
68 coal emissions have declined steadily in Europe and North America owing to the legislation
69 and effective environmental policies to reduce local anthropogenic emissions of aerosol and



70 precursor gases (Smith et al., 2011). In contrast to North America and Europe, the coal
71 consumption in China and India has experienced a substantial increase and anthropogenic
72 emissions from these regions continued to rise (Hoesly et al., 2018; Lim et al., 2020). Zheng et
73 al. (2018) also reported that due to active clean air policies and the emission control of power
74 plants and industry, anthropogenic emissions of PM_{2.5} (particulate matter less than 2.5 µm in
75 diameter) from China have significantly decreased by 33% during 2013–2017. However,
76 countries in South Asia still rely on coal and petroleum and thus aerosol emissions from South
77 Asia have kept increasing in recent years (Li et al., 2017).

78 Regional aerosol pollution can be induced by both local emissions and long-range
79 transport of pollutants across regions, countries or even continents, which impose a far-
80 reaching impact on air quality and human health (Akimoto, 2003; Anenberg et al., 2014; Jaffe
81 et al., 1999; Lin et al., 2014; Liu et al., 2009; Zhang et al., 2017). Studies reported that the air
82 quality in Europe is largely impacted by the long-range aerosol transport from North America
83 (Stohl and Trickl, 1999; Yang et al., 2018a, 2020b). Asian anthropogenic emissions in spring
84 also have a significant effect on the aerosol concentrations in North America (Jaffe et al.,
85 1999). Moreover, studies found that air pollution from Africa and Europe moved eastward and
86 merged with Asian pollution, affecting air quality in western North America (Liu et al., 2005;
87 Chin et al., 2007). Yang et al. (2017) also found that remote sources contributed the most to
88 the regions with low emissions through long-range transport, which further impacted the local
89 climate. Therefore, relying on the domestic emission control alone may be insufficient to
90 prevent air pollution due to the long-distance transport of air pollutants (Liu et al., 2009). A
91 study revealed that approximately 12% of global premature deaths caused by PM_{2.5} were



92 related to non-local air pollutants (Zhang et al., 2017). About 16% of premature deaths in India
93 caused by PM_{2.5} were attributed to aerosol transport from external source regions (David et al.,
94 2019). Within each emission source region, aerosols also come from different emission sectors.
95 Many scientific control measures and policies are implemented based on the source attribution
96 of air pollutants from individual sectors. Hence, it is of great significance to quantify source
97 contributions of long-range transport of aerosols from major emission regions of the world as
98 well as aerosols from major emission sectors.

99 Anthropogenic emissions of aerosols and precursor gases have changed significantly in
100 different source regions over the past century. Few studies focus on the source attributions of
101 aerosols across the globe over such a long period of time. In this study, we focus on the changes
102 in aerosols and emission source region and sector contributions in major source regions (i.e.,
103 North America, Europe, East Asia, South Asia) during the three important periods of emission
104 changes since industrialization (1850–1980, 1980–2010 and 2010–2017) based on the
105 Energy Exascale Earth System Model version 1 (E3SMv1), equipped with an explicit aerosol
106 source tagging system (E3SMv1-EAST).

107 **2. Methods**

108 **2.1. Model description and experimental design**

109 To study variations in historical anthropogenic aerosols in the major source regions, the
110 E3SMv1 developed by US Department of Energy (DOE) (Golaz et al., 2019) is used in this
111 study. E3SMv1 consists of atmosphere, land surface, ocean, sea ice, and river model
112 components. Aerosol microphysics and interactions with stratiform clouds are treated with the
113 four-mode Modal Aerosols Module (MAM4) (Liu et al., 2016), which predicts the mass and



114 number concentrations of sulfate, black carbon (BC), primary organic matter (POM),
115 secondary organic aerosol (SOA), marine organic aerosol, mineral dust and sea salt (Wang et
116 al., 2020). EAMv1 applies the “Morrison and Gettelman version 2” (MG2) two-moment bulk
117 microphysics parameterization for stratiform clouds (Gettelman and Morrison, 2015). It allows
118 aerosol-cloud interactions in all stratiform and shallow convective clouds but neglects in deep
119 convective clouds (Rasch et al., 2019). Liquid cloud drop activation is based on Abdul-Razzak
120 and Ghan (2000) and a classical nucleation theory-based ice nucleation parameterization for
121 the heterogeneous ice formation in mixed-phase clouds follows Y. Wang et al. (2014).
122 Hygroscopicity are specified for soluble aerosols to calculate the particle size based on relative
123 humidity. The aerosols are assumed to mix internally in the same aerosol mode and externally
124 between modes when calculating the aerosol optical properties (Ghan and Zaveri, 2007). In
125 this study, the model is configured at its standard horizontal spatial resolution of approximately
126 1° with 72 vertical layers.

127 Global emissions of aerosols and precursor gases used in the simulations are obtained
128 from the CMIP6 (the Coupled Model Intercomparison Project Phase 6) datasets (Hoesly et al.,
129 2018; van Marle et al., 2017). However, the anthropogenic emissions in China are replaced
130 with MEIC (Multi-resolution Emission Inventory for China) inventory, which fully considers
131 the implementation of clean air actions over China since the 2010s (Gao et al., 2022, 2023; Li
132 et al., 2021; Zheng et al., 2018). Following previous studies (Ren et al., 2021; Yang et al.,
133 2018a), the near-surface concentrations of PM_{2.5} here are estimated as the sum of sulfate, BC,
134 POM and SOA concentrations. Effective radiative forcing (ERF) refers to the change of the
135 net radiative flux at the top of the atmosphere (TOA) after the external forcing is applied. In



136 this study, ERF due to aerosol-radiation interactions (ERF_{ari}) for the individual tagged source
137 regions is derived as the difference in TOA net radiative fluxes from a pair of diagnostic
138 radiation calculations with and without the particular tagged aerosols from the source regions
139 for the all-sky condition following Ghan (2013).

140 This study focuses on the variations in source region and sector contributions in four major
141 emission regions of the world (North America, Europe, East Asia and South Asia) during the
142 three key historical periods of emission changes (1850–1980, 1980–2010 and 2010–2017).
143 Four simulations with monthly anthropogenic emissions of aerosols and precursors fixed at the
144 1850, 1980, 2010 and 2017 levels, respectively, are conducted. All simulations are performed
145 for one year following 6-month model spin-up. Greenhouse gas concentrations, solar insolation,
146 sea surface temperature and sea ice extent are prescribed at the 2000 levels. The meteorological
147 fields including 3-dimensional temperature, specific humidity, and winds are nudged toward
148 the MERRA-2 (Modern-Era Retrospective Analysis for Research and Applications, version 2)
149 reanalysis (Gelaro et al., 2017) in year 2017 at a 6-hourly relaxation timescale.

150 **2.2. Explicit aerosol source tagging system**

151 To examine the source-receptor relationships of aerosols, we implemented the Explicit
152 Aerosol Source Tagging (EAST) in E3SMv1. The tagging system follows the BC source-
153 tagging technique introduced in H. Wang et al. (2014), sulfate source-tagging method used in
154 Yang et al. (2017) and other carbonaceous aerosol-tagging applied in Yang et al. (2018a),
155 which was previously implemented in the Community Atmosphere Model version 5 (CAM5-
156 EAST). In E3SMv1-EAST, all the physical, chemical and dynamical processes of aerosols and



157 their precursor gases from individual source regions and sectors are simulated independently
158 by introducing additional aerosol-related variables.

159 In this study, totally 18 tags are set for each anthropogenic species of aerosols and
160 precursors. Each of the 4 major source regions, including North America (NAM), Europe
161 (EUR), East Asia (EAS) and South Asia (SAS), has 4 tags for the energy transformation and
162 extraction (ENE), industrial combustion and processes (IND), residential, commercial and
163 other (RCO) and the rest of anthropogenic emission sectors (RST). One tag is assigned to the
164 anthropogenic emissions from rest of the world (ROW) and the last tag is allocated for all the
165 natural/biogenic sources including open biomass burning, volcanic emissions and oceanic
166 emissions.

167 **2.3. Model evaluation**

168 In order to evaluate the performance of E3SMv1 in reproducing the aerosol concentrations,
169 Fig. 2 compares the simulated near-surface $PM_{2.5}$ concentrations with the observations from
170 the Interagency Monitoring of Protected Visual Environments (IMPROVE) over the U.S., the
171 European Monitoring and Evaluation Programme (EMEP) over Europe and the China National
172 Environmental Monitoring Center (CNEMC) over China in year 2017. The model successfully
173 reproduces the spatial distribution of $PM_{2.5}$ concentrations, with relatively high concentrations
174 in eastern China and low concentrations in the U.S. and Europe. The spatial correlation
175 coefficient (R) between the E3SMv1 simulated $PM_{2.5}$ concentrations and observations is +0.80.
176 The model well reproduces the $PM_{2.5}$ concentrations in the U.S. with the normalized mean
177 biases (NMB) of -11%. However, it largely underestimates the $PM_{2.5}$ concentrations in China
178 and Europe, which has also been revealed in several studies (e.g., Gao et al., 2023; Zeng et al.,



179 2021). This discrepancy is partly because E3SMv1 only considers limited aerosol species (BC,
180 POM, SOA and sulfate) without including nitrate and ammonium aerosols in the aerosol
181 module. On the other hand, the overestimated wet scavenging at the mid- and high latitudes
182 and underestimated gas-to-particle conversion can also lead to the low bias (Zeng et al., 2021).

183 **3. Results**

184 **3.1. Historical changes in aerosols over major source regions**

185 Figure 3 shows the variations in anthropogenic emissions of sulfur dioxide (SO₂) during
186 the three key periods of historical emission changes from the tagged source regions. Since
187 industrialization, anthropogenic SO₂ emissions had rising trends during 1850–1980, especially
188 in Europe and North America. Due to the implementation of clean air actions in western
189 countries, SO₂ emissions in North America and Europe declined considerably during 1980–
190 2010, while the emissions in East Asia and South Asia continued to increase. After 2010, China
191 issued several clean air policies, which led to significant decreases in anthropogenic SO₂
192 emissions in East Asia, while the SO₂ emissions in South Asia kept increasing during 2010–
193 2017. The changes in anthropogenic BC and organic carbon (OC) emissions are similar to those
194 of SO₂ (shown in Figure S1 and S2).

195 The changes in near-surface mass concentrations (Fig. 4) and column burdens (Fig. 5) of
196 anthropogenic PM_{2.5} contributed by the tagged source regions during the focused three
197 historical time periods follow the corresponding changes in anthropogenic emissions. Local
198 anthropogenic emission changes drove the PM_{2.5} to reach its peak in 1980 in North America
199 and Europe and then to decrease. The maximum PM_{2.5} appeared in 2010 in East Asia and the
200 anthropogenic PM_{2.5} level continued growing in South Asia during 1850–2017.



201 To explore which aerosol species contributed the most to the changes in $PM_{2.5}$ during the
202 focused three historical time periods, Figs. 6 and 7 illustrate the relative contributions of
203 individual aerosols to the simulated changes in near-surface $PM_{2.5}$ mass concentrations and
204 column burdens, respectively, in four major emission regions. In general, the historical changes
205 in anthropogenic $PM_{2.5}$ were primarily driven by the changes in sulfate. In North America, the
206 contribution of sulfate to near-surface $PM_{2.5}$ concentration (column burden) rose from 7%
207 (11%) in 1850 to 67% (81%) in 1980, then dropped to 52% (67%) in 2017. In Europe, sulfate
208 contribution changed from 24% (34%) in 1850 to 71% (85%) in 1980, then decreased to 50%
209 (68%) in 2017. In East Asia, sulfate contribution changes from 2% (6%) in 1850 to 51% (71%)
210 in 1980, then decreased to 33% (56%) in 2017. It is interesting that the $PM_{2.5}$ levels in East
211 Asia increased during 1980–2010, but the sulfate contribution decreased in this time period. It
212 is because the carbonaceous aerosols increased remarkably, which reduced the fractional
213 contribution of sulfate. The sulfate contribution to $PM_{2.5}$ concentration (column burden)
214 increased throughout the period of 1850–2017, from 2% (5%) to 42% (62%) in South Asia.
215 Note that the carbonaceous aerosols, especially POM, dominated the $PM_{2.5}$ in all four targeted
216 regions in 1850, resulting from the high heating demand from the residential sector.

217 **3.2 Changes in contributions from major source regions and sectors**

218 Figure 8 shows the relative contributions from local and remote anthropogenic sources to
219 the near-surface concentrations and column burdens of $PM_{2.5}$ in the four targeted regions in
220 2010. Local sources dominated the near-surface anthropogenic $PM_{2.5}$ concentrations over the
221 high emission regions including eastern China, eastern U.S. and Indo-Gangetic Plain, with
222 local contributions being higher than 90%. In the regions with low emissions, such as the



223 Tibetan Plateau, the anthropogenic $PM_{2.5}$ concentrations were largely contributed by the long-
224 range transport of aerosols. The spatial distributions of burden contribution are similar to those
225 of corresponding contribution near the surface, but the long-range transport contributed more
226 to the column burden than to the near-surface contribution due to the more efficient pollutant
227 transport in the free troposphere than within the boundary layer. The long-range transport
228 contributes 30%–35% of $PM_{2.5}$ burden in East Asia and South Asia and 50–55% in North
229 America and Europe, much higher than the 10%–25% for the near-surface concentrations over
230 the four targeted regions.

231 Since both local and remote emissions can contribute to the anthropogenic $PM_{2.5}$, it is
232 valuable to know the historical changes in these contributions, especially by the local sources
233 from individual emission sectors and by remote sources from major emission regions. Figure
234 9 illustrates changes in the local source contributions from major emission sectors to the near-
235 surface concentrations and column burdens of $PM_{2.5}$ during 1850–2017. In North America and
236 Europe, the historical changes in anthropogenic $PM_{2.5}$ were largely induced by changes in
237 emissions from the local energy (ENE) sector, followed by the industry (IND) sector, which
238 increased before 1980 and decreased afterward. In East Asia, ENE, IND and residential (RCO)
239 sector emissions all had significant contributions to the increases in $PM_{2.5}$ concentration and
240 burden from 1850 to 1980. Then the contribution from local IND sector showed the largest
241 increases from 1980 to 2010 and decreases from 2010 to 2017. In South Asia, the
242 anthropogenic $PM_{2.5}$ increases from 1850 to 1980 were mainly attributed to the RCO emission
243 increases. After that, increases in ENE emissions dominated the rising $PM_{2.5}$ levels in South
244 Asia during 1980–2017.



245 Figure 10 presents changes in remote emission contributions from the tagged source
246 regions to the column burdens of PM_{2.5} during 1850–2017. The contributions from long-range
247 transport to the near-surface concentrations and their historical variations over the four major
248 emissions regions are relatively small, which were also reported in previous studies (e.g., Yang
249 et al., 2018b) and are not discussed here. During 1850–1980, the long-range transport
250 contributions to the PM_{2.5} burdens show increases and the contributions from ROW increased
251 the most among the tagged source regions over all four targeted receptor regions. Note that
252 aerosol emissions from North America contributed to the increase in European PM_{2.5} burden
253 by 1.7 mg m⁻² and sources from Europe were also responsible for the PM_{2.5} burden increase by
254 1.0 mg m⁻² in East Asia and 1.1 mg m⁻² in South Asia. During 1980–2010, the long-range
255 transport from North America and Europe decreased, but that from East Asia and South Asia
256 increased. East Asia contributed 0.4–0.6 mg m⁻² to the PM_{2.5} burden increases in North
257 America, while Europe and South Asia contributed about 0.3 mg m⁻². In East Asia, 1.6 mg m⁻²
258 of the PM_{2.5} burden increase was attributed to South Asian sources and 0.8 mg m⁻² of the
259 PM_{2.5} burden increase in South Asia during this time period was due to increases in East Asian
260 emissions. From 2010 to 2017, owing to the clean air actions in China, contributions from East
261 Asia to the PM_{2.5} burdens in the other three targeted regions decreased by 0.3–0.6 mg m⁻².
262 However, due to the continuous increases in South Asian emissions, South Asia still
263 contributed to the PM_{2.5} burden increase in East Asia by 0.4 mg m⁻² during this short time
264 period.

265 3.3 Changes in effective radiative forcing due to aerosol-radiation interactions



266 The variation in aerosols can have a significant impact on ERF through aerosol-radiation
267 and aerosol-cloud interactions. Figure 11 shows changes in ERF due to aerosol-radiation
268 interactions (ERF_{ari}) at the top of the atmosphere (TOA) that can be attributed to changes in
269 anthropogenic emissions from the tagged regions in the three key periods during 1850–2017.
270 Due to the increases in aerosols from 1850 to 1980, a large negative ERF_{ari} was located over
271 the major source regions and their downwind areas, with maximum ERF_{ari} changes being larger
272 than 2 W m^{-2} over eastern U.S., Europe and eastern China. In 2010, there were positive ERF_{ari}
273 changes (warming effect) by a maximum of 2 W m^{-2} in North America and Europe compared
274 to 1980, which were due to the decreases in anthropogenic aerosols in these two regions. The
275 positive ERF_{ari} changes due to the decrease in North American aerosols extended across the
276 North Atlantic and caused an increase in incoming radiation by up to 0.5 W m^{-2} in Europe.
277 Similarly, the decrease in aerosols from Europe also led to a positive ERF_{ari} change by up to
278 0.5 W m^{-2} in the downwind regions including Russia and northern China during 1980–2010.
279 Increases in aerosols in China during 1980–2010 and decreases during 2010–2017 produced
280 negative (cooling) and positive (warming) changes in ERF_{ari} , respectively, over eastern China
281 and North Pacific, which largely contradicted each other. The continuously growing aerosols
282 in South Asia induced negative ERF_{ari} changes (cooling) in South Asia, Southeast Asia and
283 southern China during both 1980–2010 and 2010–2017. Note that in this study we only
284 quantify the ERF_{ari} for the major emission regions based on the source tagging technique. The
285 quantification of ERF due to aerosol-cloud interactions (ERF_{aci}) requires additional simulations,
286 which could be further examined in future studies.

287 **4. Conclusions and Discussions**



288 Since the start of industrialization, aerosols have changed significantly in different regions
289 of the world driven by global economic development and air pollution control measures. It is
290 of great significance to quantify the contributions of aerosols from major emission source
291 regions and sectors during the key periods of substantial emission changes. In this study, the
292 Explicit Aerosol Source Tagging (EAST) technique is implemented in E3SMv1 to quantify the
293 variations in the concentrations, source contributions, and the subsequent effective radiative
294 forcing of anthropogenic aerosols in four major source regions (NAM, EUR, EAS and SAS)
295 during three key historical periods of emission changes (1850–1980, 1980–2010 and 2010–
296 2017).

297 Following the corresponding anthropogenic emission changes, $PM_{2.5}$ concentrations
298 reached its peak in 1980 in North America and Europe, while the peak of $PM_{2.5}$ in East Asia
299 occurred in 2010. The $PM_{2.5}$ from anthropogenic sources in South Asia continued growing
300 during 1850–2017. These changes in anthropogenic $PM_{2.5}$ were primarily dominated by
301 changes in sulfate aerosol. In North America and Europe, historical changes in anthropogenic
302 $PM_{2.5}$ were mainly caused by changes in emissions from local energy sector, followed by the
303 industrial sector, which increased from 1850 to 1980 and decreased afterward. In East Asia,
304 energy, industrial, and residential emissions contributed significantly to the increase in $PM_{2.5}$
305 from 1850 to 1980, then the local industrial sector caused the most increase from 1980 to 2010,
306 and declined from 2010 to 2017. For South Asia, the increase in $PM_{2.5}$ was mainly due to
307 emission changes in the residential sector from 1850 to 1980, then the increase in energy-
308 related emissions became dominant to the rise of $PM_{2.5}$ levels during 1980–2017.



309 Regional aerosol pollution comes from both local emissions and long-range transport of
310 remote emissions. Local emissions contribute the most in regions with high emissions, while
311 in regions with low emissions the long-distance transport plays an important role. Due to the
312 more efficient transport of air pollutants in the free troposphere, contributions of long-range
313 transport to column burden are greater than to the near-surface concentration over all four
314 targeted receptor regions. From 1850 to 1980, increases in emissions from North America
315 contributed to the increase in European $\text{PM}_{2.5}$ burden by 1.7 mg m^{-2} and emissions from Europe
316 were also responsible for the $\text{PM}_{2.5}$ burden increase by 1.0 mg m^{-2} in East Asia and 1.1 mg m^{-2}
317 in South Asia. From 1980 to 2010, the long-range transport from North America and Europe
318 decreased, while those from East Asia and South Asia increased. East Asia contributed 0.4--
319 0.6 mg m^{-2} to the $\text{PM}_{2.5}$ burden increases in North America, while Europe and South Asia
320 contributed about 0.3 mg m^{-2} . In East Asia, 1.6 mg m^{-2} of the $\text{PM}_{2.5}$ burden increase was
321 attributed to South Asian sources and 0.8 mg m^{-2} of the $\text{PM}_{2.5}$ burden increase in South Asia
322 during this time period was due to the increases in East Asian emissions. From 2010 to 2017,
323 the contributions from East Asia to the $\text{PM}_{2.5}$ burdens in the other three targeted regions
324 declined by $0.3\text{--}0.6 \text{ mg m}^{-2}$ due to Clean Air actions in China. However, due to the continuous
325 increase of emissions in South Asia, the $\text{PM}_{2.5}$ burden in East Asia still increased by 0.4 mg m^{-2} .
326

327 Changes in aerosols can have a significant impact on ERF, which further imposes an
328 impact on climate. Large negative ERF_{ari} appeared over the major source regions and their
329 downwind areas during 1850–1980 due to the increases in aerosol emissions, with maximum
330 ERF_{ari} changes being larger than 2 W m^{-2} over eastern North America, Europe and eastern



331 China. From 1980 to 2010, a positive ERF_{ari} change caused by a decline in North American
332 aerosols extended over the North Atlantic, resulting in a warming of up to 0.5 W m^{-2} in Europe.
333 Meanwhile, a decline of aerosols in Europe also caused a warming of up to 0.5 W m^{-2} in Russia
334 and northern China. The changes in ERF_{ari} from the increase (from 1980 to 2010) and decrease
335 (from 2010 to 2017) of aerosols in China had an opposite sign. The continuous aerosol
336 increases in South Asia from 1980 to 2017 resulted in negative ERF_{ari} changes in South Asia,
337 Southeast Asia, and southern China.

338 This study provides an in-depth analysis of historical changes in anthropogenic aerosol
339 concentrations, compositions, source contributions and radiative impacts in the four major
340 emission source regions of the globe, which has important implications for the pollution
341 prevention/control measures and decision making for global collaboration. The spatial
342 distribution and changes in anthropogenic aerosols are similar to those reported in previous
343 studies (Hoesly, et al., 2018; Lim, et al., 2020). However, we also note that the E3SMv1 model
344 underestimates the near-surface $PM_{2.5}$ concentrations in Europe and East Asia, which could
345 lead to an underestimate of the corresponding radiative and climate impact. Our analysis
346 focuses on aerosols from anthropogenic emissions; however, with the increasing attention to
347 air quality in many countries around the world, anthropogenic aerosol concentrations are
348 declining and contributions from biomass burning aerosols are becoming more and more
349 important. The source contributions and impacts of biomass burning aerosols will be
350 investigated in our future work. Also, this study only quantifies the ERF_{ari} for individual major
351 emission regions based on the source tagging technique and radiation diagnostic calculations.



352 The quantification of ERF_{aci} requires additional simulations, which could be further examined

353 in future studies.



354 **Author contributions.** YY designed the research, added the tagging code and performed
355 simulations; SM analyzed the data. All authors including HW, PW, and HL discussed the
356 results and wrote the paper.

357

358 **Code and data availability.** The E3SMv1 model is available at <https://github.com/E3SM->
359 [Project/E3SM](https://github.com/E3SM-Project/E3SM)(last access:1 October 2022) (<https://doi.org/10.11578/E3SM/dc.20180418.36>;
360 E3SM Project, 2018). Our results can be made available upon request.

361

362 **Acknowledgments.** HW acknowledges the support by the U.S. Department of Energy (DOE),
363 Office of Science, Office of Biological and Environmental Research (BER), as part of the
364 Earth and Environmental System Modeling program. The Pacific Northwest National
365 Laboratory (PNNL) is operated for DOE by the Battelle Memorial Institute under contract
366 DE-AC05-76RLO1830.

367

368 **Financial support.** This study was supported by the National Key Research and
369 Development Program of China (grant 2020YFA0607803 and 2019YFA0606800), the
370 National Natural Science Foundation of China (grant 41975159), Jiangsu Science Fund for
371 Distinguished Young Scholars (grant BK20211541), and the Jiangsu Science Fund for
372 Carbon Neutrality (grant no. BK20220031).

373

374 **Conflict of interest.**

375 At least one of the (co-)authors is a member of the editorial board of ACP.



376 **References**

377

378 Abdul-Razzak, H. and Ghan, S. J.: A parameterization of aerosol activation, 2. Multiple
379 aerosol types, *J. Geophys. Res.*, 105, 6837–6844,
380 <https://doi.org/10.1029/1999JD901161>, 2000.

381

382 Akimoto, H.: Global Air Quality and Pollution, *Science*, 302, 1716–1719,
383 <https://doi.org/10.1126/science.1092666>, 2003.

384

385 Anenberg, S. C., Horowitz, L. W., Tong, D. Q., and West, J. J.: An Estimate of the Global
386 Burden of Anthropogenic Ozone and Fine Particulate Matter on Premature Human
387 Mortality Using Atmospheric Modeling, *Environ. Health Perspect.*, 118, 1189–1195,
388 <https://doi.org/10.1289/ehp.0901220>, 2010.

389

390 Anenberg, S. C., West, J. J., Yu, H., Chin, M., Schulz, M., Bergmann, D., Bey, I., Bian, H.,
391 Diehl, T., Fiore, A., Hess, P., Marmer, E., Montanaro, V., Park, R., Shindell, D.,
392 Takemura, T., and Dentener, F.: Impacts of intercontinental transport of anthropogenic
393 fine particulate matter on human mortality, *Air. Qual. Atmos. Health.*, 7, 369–379,
394 <https://doi.org/10.1007/s11869-014-0248-9>, 2014.

395

396 Carslaw, K. S., Gordon, H., Hamilton, D. S., Johnson, J. S., Regayre, L. A., Yoshioka, M.,
397 and Pringle, K. J.: Aerosols in the Pre-industrial Atmosphere, *Curr. Clim. Change Rep.*,
398 3, 1–15, <https://doi.org/10.1007/s40641-017-0061-2>, 2017.

399

400 Chen, D., Liao, H., Yang, Y., Chen, L., and Wang, H.: Simulated aging processes of black
401 carbon and its impact during a severe winter haze event in the Beijing-Tianjin-Hebei
402 region, *Sci. Total Environ.*, 755, 142712,
403 <https://doi.org/10.1016/j.scitotenv.2020.142712>, 2021.

404

405 Chin, M., Diehl, T., Ginoux, P., and Malm, W.: Intercontinental transport of pollution and
406 dust aerosols: implications for regional air quality, *Atmos. Chem. Phys.*, 7, 5501–5517,
407 <https://doi.org/10.5194/acp-7-5501-2007>, 2007.

408

409 David, L. M., Ravishankara, A. R., Kodros, J. K., Pierce, J. R., Venkataraman, C., and
410 Sadavarte, P.: Premature mortality due to PM_{2.5} over India: Effect of atmospheric
411 transport and anthropogenic emissions, *Geohealth*, 3, 2–10,
412 <https://doi.org/10.1029/2018GH000169>, 2019.

413

414 Finlayson-Pitts, B. J., and Pitts, J. N.: Tropospheric Air Pollution: Ozone, Airborne Toxics,
415 Polycyclic Aromatic Hydrocarbons, and Particles, *Science*, 276, 1045–1051,
416 <https://doi.org/10.1126/science.276.5315.1045>, 1997.

417

418 Gao, J., Yang, Y., Wang, H., Wang, P., Li, H., Li, M., Ren, L., Yue, X., and Liao, H.: Fast
419 climate responses to emission reductions in aerosol and ozone precursors in China



- 420 during 2013–2017, *Atmos. Chem. Phys.*, 22, 7131–7142, [https://doi.org/10.5194/acp-](https://doi.org/10.5194/acp-22-7131-2022)
421 [22-7131-2022](https://doi.org/10.5194/acp-22-7131-2022), 2022.
- 422
- 423 Gao, J., Yang, Y., Wang, H., Wang, P., Li, B., Li, J., Wei, J., Gao, M., and Liao, H.: Climate
424 responses in China to domestic and foreign aerosol changes due to clean air actions
425 during 2013–2019, *npj Clim. Atmos. Sci.*, 6, 160, [https://doi.org/10.1038/s41612-023-](https://doi.org/10.1038/s41612-023-00488-y)
426 [00488-y](https://doi.org/10.1038/s41612-023-00488-y), 2023.
- 427
- 428 Gelaro, R., McCarty, W., Suárez, M. J., Todling, R., Molod, A., Takacs, L., Randles, C. A.,
429 Darmenov, A., Bosilovich, M. G., Reichle, R., Wargan, K., Coy, L., Cullather, R.,
430 Draper, C., Akella, S., Buchard, V., Conaty, A., da Silva, A. M., Gu, W., Kim, G.,
431 Koster, R., Lucchesi, R., Merkova, D., Nielsen, J. E., Partyka, G., Pawson, S., Putman,
432 W., Rienecker, M., Schubert, S. D., Sienkiewicz, M., and Zhao, B.: The Modern-Era
433 Retrospective Analysis for Research and Applications, Version 2 (MERRA-2), *J.*
434 *Climate*, 30, 5419–5454, <https://doi.org/10.1175/JCLI-D-16-0758.1>, 2017.
- 435
- 436 Ghan, S. J.: Technical Note: Estimating aerosol effects on cloud radiative forcing, *Atmos.*
437 *Chem. Phys.*, 13, 9971–9974, <https://doi.org/10.5194/acp-13-9971-2013>, 2013.
- 438
- 439 Ghan, S. J. and Zaveri, R. A.: Parameterization of optical properties for hydrated internally
440 mixed aerosol, *J. Geophys. Res.-Atmos.*, 112, D10201,
441 <https://doi.org/10.1029/2006JD007927>, 2007.
- 442
- 443 Golaz, J. C., Caldwell, P. M., Van Roekel, L. P., Petersen, M. R., Tang, Q., Wolfe, J. D.,
444 Abeshu, G., Anantharaj, V., Asay-Davis, X. S., Bader, D. C., Baldwin, S. A., Bisht, G.,
445 Bogenschutz, P. A., Branstetter, M., Brunke, M. A., Brus, S. R., Burrows, S. M.,
446 Cameron-Smith, P. J., Donahue, A. S., Deakin, M., Easter, R. C., Evans, K. J., Feng, Y.,
447 Flanner, M., Foucar, J. G., Fyke, J. G., Griffin, B. M., Hannay, C., Harrop, B. E.,
448 Hoffman, M. J., Hunke, E. C., Jacob, R. L., Jacobsen, D. W., Jeffery, N., Jones, P. W.,
449 Keen, N. D., Klein, S. A., Larson, V. E., Leung, L. R., Li, H. Y., Lin, W., Lipscomb, W.
450 H., Ma, P., Mahajan, S., Maltrud, M. E., Mametjanov, A., McClean, J. L., McCoy, R.
451 B., Neale, R. B., Price, S. F., Qian, Y., Rasch, P. J., Eyre, J. E. J. R., Riley, W. J.,
452 Ringer, T. D., Roberts, A. F., Roesler, E. L., Salinger, A. G., Shaheen, Z., Shi, X.,
453 Singh, B., Tang, J., Taylor, M. A., Thornton, P. E., Turner, A. K., Veneziani, M., Wan,
454 H., Wang, H., Wang, S., Williams, D. N., Wolfram, P. J., Worley, P. H., Xie, S., Yang
455 Y., Yoon, J., Zelinka, M. D., Zender, C. S., Zeng, X., Zhang, C., Zhang, K., Zhang, Y.,
456 Zheng, X., Zhou, T., and Zhu, Q.: The DOE E3SM Coupled Model Version 1:
457 Overview and Evaluation at Standard Resolution, *J. Adv. Model. Earth Syst.*, 11, 2089–
458 2129. <https://doi.org/10.1029/2018MS001603>, 2019.
- 459
- 460 Hoesly, R. M., Smith, S. J., Feng, L., Klimont, Z., Janssens-Maenhout, G., Pitkanen, T.,
461 Seibert, J. J., Vu, L., Andres, R. J., Bolt, R. M., Bond, T. C., Dawidowski, L., Kholod,
462 N., Kurokawa, J., Li, M., Liu, L., Lu, Z., Moura, M. C. P., O'Rourke, P. R., and Zhang,
463 Q.: Historical (1750–2014) anthropogenic emissions of reactive gases and aerosols from



- 464 the Community Emissions Data System (CEDS), *Geosci. Model Dev.*, 11, 369–408,
465 <https://doi.org/10.5194/gmd-11-369-2018>, 2018.
- 466
- 467 Jaffe, D., Anderson, T., Covert, D., Kotchenruther, R., Trost, B., Danielson, J., Simpson, W.,
468 Berntsen, T., Karlsdottir, S., Blake, D., Harris, J., Carmichael, G., and Uno, I.: Transport
469 of Asian air pollution to North America, *Geophys. Res. Lett.*, 26, 711–714,
470 <https://doi.org/10.1029/1999GL900100>, 1999.
- 471
- 472 Li, C., McLinden, C., Fioletov, V., Krotkov, N., Carn, S., Joiner, J., Streets, D., He, H., Ren,
473 X., Li, Z., and Dickerson, R.: India Is Overtaking China as the World’s Largest Emitter
474 of Anthropogenic Sulfur Dioxide, *Sci. Rep.*, 7, 14304, <https://doi.org/10.1038/s41598-017-14639-8>, 2017.
- 475
- 476
- 477 Li, H., Yang, Y., Wang, H., Li, B., Wang, P., Li, J., and Liao, H.: Constructing a
478 spatiotemporally coherent long-term PM_{2.5} concentration dataset over China using a
479 machine learning approach, *Sci. Total Environ.*, 765, 144263,
480 <https://doi.org/10.1016/j.scitotenv.2020.144263>, 2021.
- 481
- 482 Liao, H., Chang, W., and Yang, Y.: Climatic effects of air pollutants over China: A review,
483 *Adv. Atmos. Sci.*, 32, 115–139, <https://doi.org/10.1007/s00376-014-0013-x>, 2015.
- 484
- 485 Lim, C.-H., Ryu, J., Choi, Y., Jeon, S. W., and Lee, W.-K.: Understanding global PM_{2.5}
486 concentrations and their drivers in recent decades (1998–2016), *Environ. Int.*, 144,
487 106011, <https://doi.org/10.1016/j.envint.2020.106011>, 2020.
- 488
- 489 Lin, J., Pan, D., Davis, S. J., Zhang, Q., He, K., Wang, C., Streets, D. G., Wuebbles, D. J.,
490 and Guan, D.: China’s international trade and air pollution in the United States, *Proc.*
491 *Natl. Acad. Sci.*, 111, 1736–1741, <https://doi.org/10.1073/pnas.1312860111>, 2014.
- 492
- 493 Liu, J., and Mauzerall, D.: Estimating the average time for inter-continental transport of air
494 pollutants, *Geophys. Res. Lett.*, 32, L11814, <https://doi.org/10.1029/2005GL022619>,
495 2005.
- 496
- 497 Liu, J., Mauzerall, D. L., Horowitz, L. W., Ginoux, P., and Fiore, A. M.: Evaluating inter-
498 continental transport of fine aerosols: (1) Methodology, global aerosol distribution and
499 optical depth, *Atmos. Environ.*, 43, 4327–4338,
500 <https://doi.org/10.1016/j.atmosenv.2009.03.054>, 2009.
- 501
- 502 Lohmann, U., and Feichter, J.: Global indirect aerosol effects: a review, *Atmos. Chem. Phys.*,
503 5, 715–737, <https://doi.org/10.5194/acp-5-715-2005>, 2005.
- 504
- 505 Lou, S., Yang, Y., Wang, H., Smith, S. J., Qian, Y., and Rasch, P. J.: Black carbon amplifies
506 haze over the North China Plain by weakening the East Asian winter monsoon,
507 *Geophys. Res. Lett.*, 46, 452–460, <https://doi.org/10.1029/2018GL080941>, 2019.



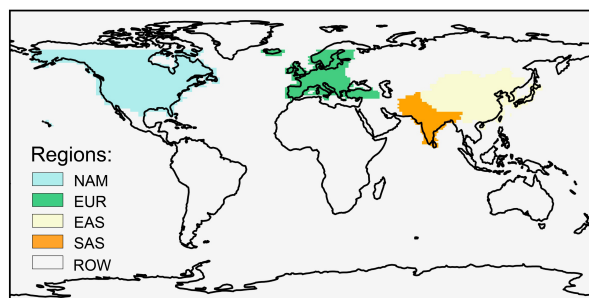
- 508
509 Rasch, P. J., Xie, S., Ma, P.-L., Lin, W., Wang, H., Tang, Q., Burrows, S. M., Caldwell, P.,
510 Zhang, K., Easter, R. C., Cameron-Smith, P., Singh, B., Wan, H., Golaz, J.-C., Harrop,
511 B. E., Roesler, E., Bacmeister, J., Larson, V. E., Evans, K. J., Qian, Y., Taylor, M.,
512 Leung, L. R., Zhang, Y., Brent, L., Branstetter, M., Hannay, C., Mahajan, S.,
513 Mامتjanov, A., Neale, R., Richter, J. H., Yoon, J.-H., Zender, C. S., Bader, D.,
514 Flanner, M., Foucar, J. G., Jacob, R., Keen, N., Klein, S. A., Liu, X., Salinger, A. G.,
515 Shrivastava, M., and Yang, Y.: An overview of the atmospheric component of the
516 Energy Exascale Earth System Model, *J. Adv. Model. Earth Sy.*, 11, 2377–2411,
517 <https://doi.org/10.1029/2019MS001629>, 2019.
518
519 Pöschl, U.: Atmospheric Aerosols: Composition, Transformation, Climate and Health
520 Effects, *Angew. Chem. Int. Ed.*, 44, 7520–7540,
521 <https://doi.org/10.1002/anie.200501122>, 2005.
522
523 Ren, L., Yang, Y., Wang, H., Wang, P., Chen, L., Zhu, J., and Liao, H.: Aerosol transport
524 pathways and source attribution in China during the COVID-19 outbreak, *Atmos. Chem.*
525 *Phys.*, 21, 15431–15445, <https://doi.org/10.5194/acp-21-15431-2021>, 2021.
526
527 Rosenfeld, D., Lohmann, U., Raga, G. B., Kulmala, M., Fuzzi, S., Reissell, A., and Andreae,
528 M. O.: Flood or Drought: How Do Aerosols Affect Precipitation?, *Science*, 321, 1309–
529 1313, <https://doi.org/10.1126/science.1160606>, 2008.
530
531 Smith, S. J., van Aardenne, J., Klimont, Z., Andres, R. J., Volke, A., and Arias, S. D.:
532 Anthropogenic sulfur dioxide emissions: 1850–2005, *Atmos. Chem. Phys.*, 11, 1101–
533 1116, <https://doi.org/10.5194/acp-11-1101-2011>, 2011.
534
535 Stohl, A., and Trickl, T.: A textbook example of long-range transport: Simultaneous
536 observation of ozone maxima of stratospheric and North American origin in the free
537 troposphere over Europe, *J. Geophys. Res.*, 104, 30445–30462,
538 <https://doi.org/10.1029/1999JD900803>, 1999.
539
540 van Marle, M. J. E., Kloster, S., Magi, B. I., Marlon, J. R., Daniau, A.-L., Field, R. D.,
541 Arneeth, A., Forrest, M., Hantson, S., Kehrwald, N. M., Knorr, W., Lasslop, G., Li, F.,
542 Mangeon, S., Yue, C., Kaiser, J. W., and van der Werf, G. R.: Historic global biomass
543 burning emissions for CMIP6 (BB4CMIP) based on merging satellite observations with
544 proxies and fire models (1750–2015), *Geosci. Model Dev.*, 10, 3329–3357,
545 <https://doi.org/10.5194/gmd-10-3329-2017>, 2017.
546
547 Wang, H., Rasch, P. J., Easter, R. C., Singh, B., Zhang, R., Ma, P.-L., Qian, Y., Ghan, S. J.,
548 and Beagley, N.: Using an explicit emission tagging method in global modeling of
549 source-receptor relationships for black carbon in the Arctic: Variations, sources, and
550 transport pathways, *J. Geophys. Res. Atmos.*, 119, 12888–12909,
551 <https://doi.org/10.1002/2014JD022297>, 2014.



- 552
553 Wang, H., Easter, R. C., Zhang, R., Ma, P.-L., Singh, B., Zhang, K., Ganguly, D., Rasch, P.
554 J., Burrows, S. M., Ghan, S. J., Lou, S., Qian, Y., Yang, Y., Feng, Y., Flanner, M.,
555 Leung, L. R., Liu, X., Shrivastava, M., Sun, J., Tang, Q., Xie, S., and Yoon, J.-H.:
556 Aerosols in the E3SM Version 1: New developments and their impacts on radiative
557 forcing, *J. Adv. Model. Earth Syst.*, 12, e2019MS001851,
558 <https://doi.org/10.1029/2019MS001851>, 2020.
559
560 Wang, Y., Liu, X., Hoose, C., and Wang, B.: Different contact angle distributions for
561 heterogeneous ice nucleation in the Community Atmospheric Model version 5, *Atmos.*
562 *Chem. Phys.*, 14, 10411–10430, <https://doi.org/10.5194/acp-14-10411-2014>, 2014.
563
564 Yang, Y., Wang, H., Smith, S. J., Easter, R., Ma, P.-L., Qian, Y., Yu, H., Li, C., and Rasch,
565 P. J.: Global source attribution of sulfate concentration and direct and indirect radiative
566 forcing, *Atmos. Chem. Phys.*, 17, 8903–8922, [https://doi.org/10.5194/acp-17-8903-](https://doi.org/10.5194/acp-17-8903-2017)
567 [2017](https://doi.org/10.5194/acp-17-8903-2017), 2017.
568
569 Yang, Y., Wang, H., Smith, S. J., Zhang, R., Lou, S., Qian, Y., Ma, P., and Rasch P. J.:
570 Recent intensification of winter haze in China linked to foreign emissions and
571 meteorology, *Sci. Rep.*, 8, 2107, <https://doi.org/10.1038/s41598-018-20437-7>, 2018a.
572
573 Yang, Y., Wang, H., Smith, S. J., Zhang, R., Lou, S., Yu, H., Li, C., and Rasch, P. J.: Source
574 Apportionments of Aerosols and Their Direct Radiative Forcing and Long-Term Trends
575 Over Continental United States, *Earth's Future*, 6, 793–808,
576 <https://doi.org/10.1029/2018EF000859>, 2018b.
577
578 Yang, Y., Ren, L., Li, H., Wang, H., Wang, P., Chen, L., Yue, X., and Hong, L.: Fast climate
579 responses to aerosol emission reductions during the COVID-19 pandemic, *Geophys.*
580 *Res. Lett.*, 47, e2020GL089788, <https://doi.org/10.1029/2020GL089788>, 2020a.
581
582 Yang, Y., Lou, S., Wang, H., Wang, P., and Liao, H.: Trends and source apportionment of
583 aerosols in Europe during 1980–2018, *Atmos. Chem. Phys.*, 20, 2579–2590,
584 <https://doi.org/10.5194/acp-20-2579-2020>, 2020b.
585
586 Yang, Y., Ren, L., Wu, M., Wang, H., Song, F., Leung, L. R., Hao, X., Li, J., Chen, L., Li,
587 H., Zeng, L., Zhou, Y., Wang, P., Liao, H., Wang, J., and Zhou, Z.-Q.: Abrupt emissions
588 reductions during COVID-19 contributed to record summer rainfall in China, *Nat.*
589 *Commun.*, 13, 959, <https://doi.org/10.1038/s41467-022-28537-9>, 2022.
590
591 Zeng, L., Yang, Y., Wang, H., Wang, J., Li, J., Ren, L., Li, H., Zhou, Y., Wang, P., and Liao,
592 H.: Intensified modulation of winter aerosol pollution in China by El Niño with short
593 duration, *Atmos. Chem. Phys.*, 21, 10745–10761, [https://doi.org/10.5194/acp-21-10745-](https://doi.org/10.5194/acp-21-10745-2021)
594 [2021](https://doi.org/10.5194/acp-21-10745-2021), 2021.
595



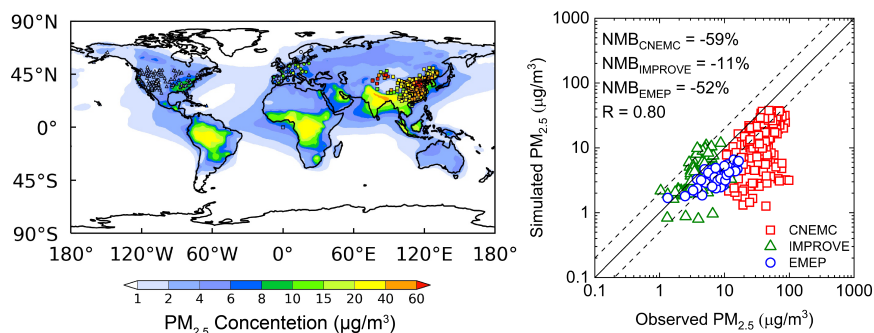
- 596 Zhang, Q., Jiang, X., Tong, D., Davis, S. J., Zhao, H., Geng, G., Feng, T., Zheng, B., Lu, Z.,
597 Streets, D. G., Ni, R., Brauer, M., van Donkelaar, A., Martin, R. V., Huo, H., Liu, Z.,
598 Pan, D., Kan, H., Yan, Y., Lin, J., He, K., and Guan, D.: Transboundary health impacts
599 of transported global air pollution and international trade, *Nature*, 543, 705–709,
600 <https://doi.org/10.1038/nature21712>, 2017.
601
- 602 Zheng, B., Tong, D., Li, M., Liu, F., Hong, C., Geng, G., Li, H., Li, X., Peng, L., Qi, J., Yan,
603 L., Zhang, Y., Zhao, H., Zheng, Y., He, K., and Zhang, Q.: Trends in China’s
604 anthropogenic emissions since 2010 as the consequence of clean air actions, *Atmos.*
605 *Chem. Phys.*, 18, 14095–14111, <https://doi.org/10.5194/acp-18-14095-2018>, 2018.
606



607

608 **Figure 1.** Tagged source regions (NAM: North America; EUR: Europe; EAS: East Asia; SAS:

609 South Asia; ROW: rest of the world).

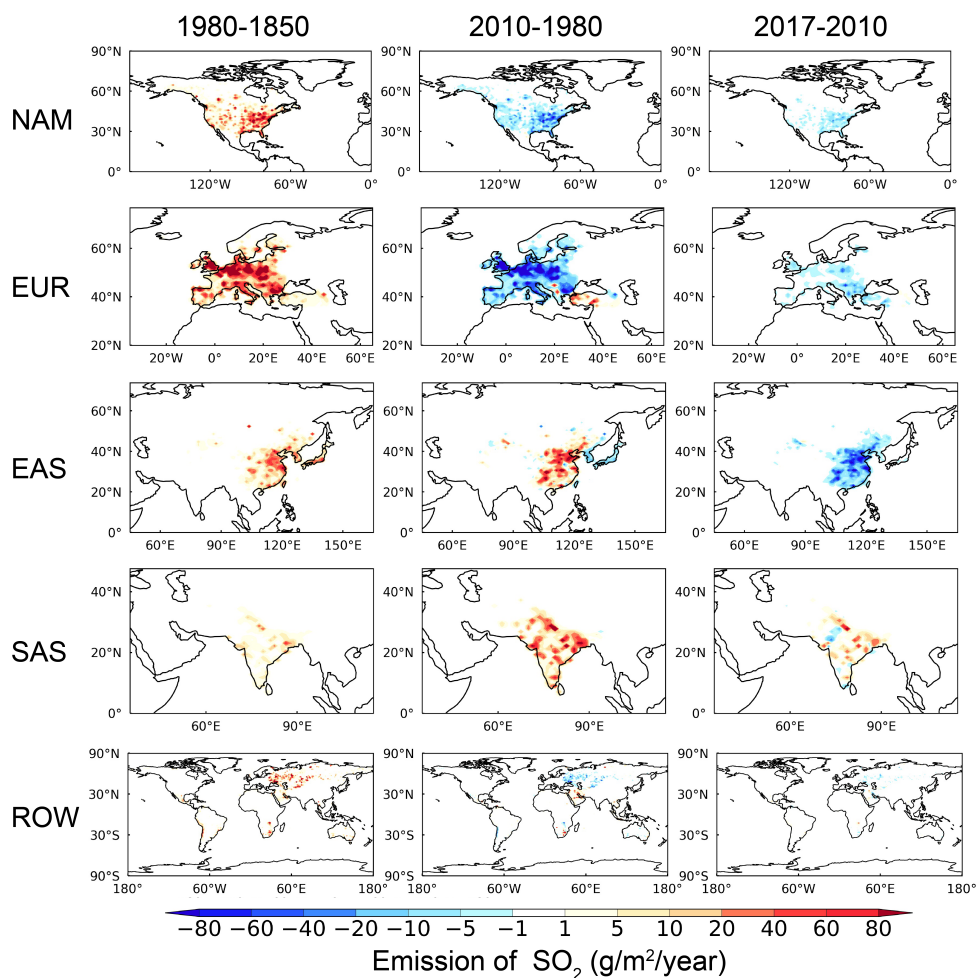


610

611 **Figure 2.** Spatial distribution (left panel) and scatter plot (right) between the simulated and
 612 observed annual mean near-surface PM_{2.5} concentrations (µg m⁻³) in 2017. Observational data
 613 are from IMPROVE (triangle), EMEP (circle) and CNEMC (square). The solid line marks the
 614 1:1 ratio and dashed lines mark the 1:2 and 2:1 ratios. Normalized mean bias (NMB) and
 615 correlation coefficient (R) between observation and simulation are shown on the right panel.
 616 $NMB = 100\% \times \frac{\sum(M_i - O_i)}{\sum O_i}$, where M_i and O_i are the modeled and observed values
 617 at site i , respectively.

618

619

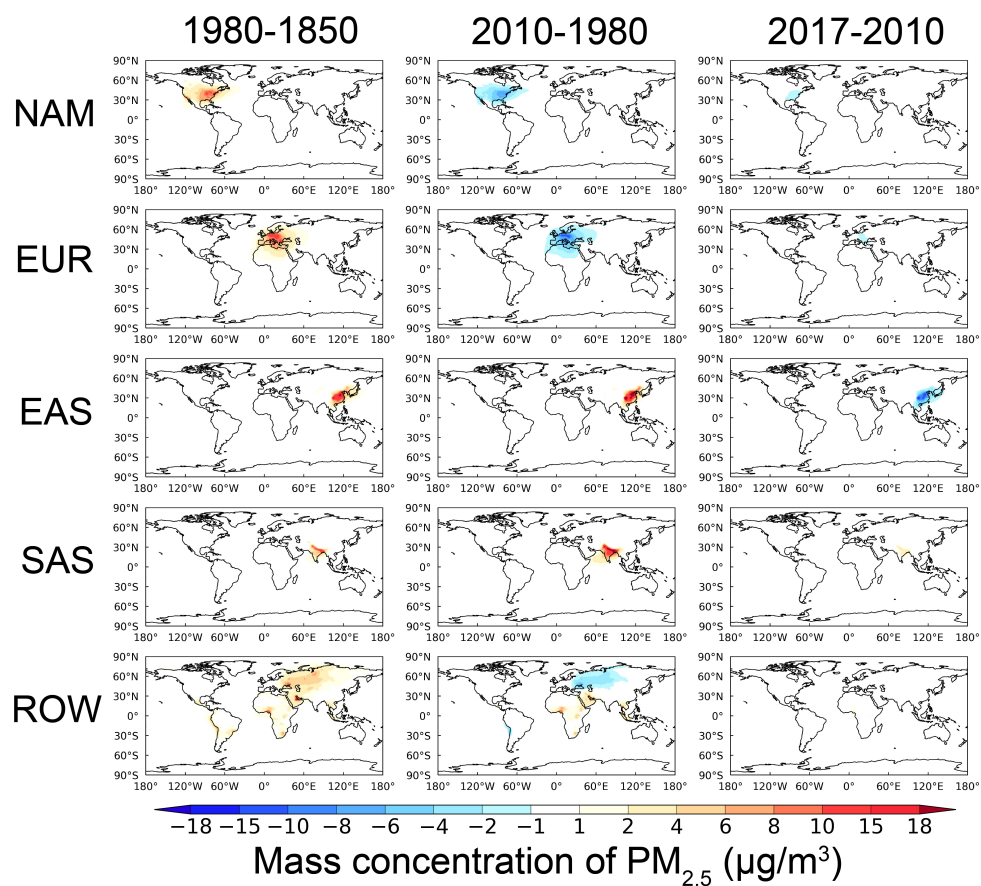


620

621 **Figure 3.** Changes in anthropogenic sulfur dioxide (SO₂) emissions (g/m²/year) between 1850
622 and 1980 (left), between 1980 and 2010 (middle), and between 2010 and 2017 (right) in the 5
623 tagged source regions (NAM, EUR, EAS, SAS and ROW from top to bottom).

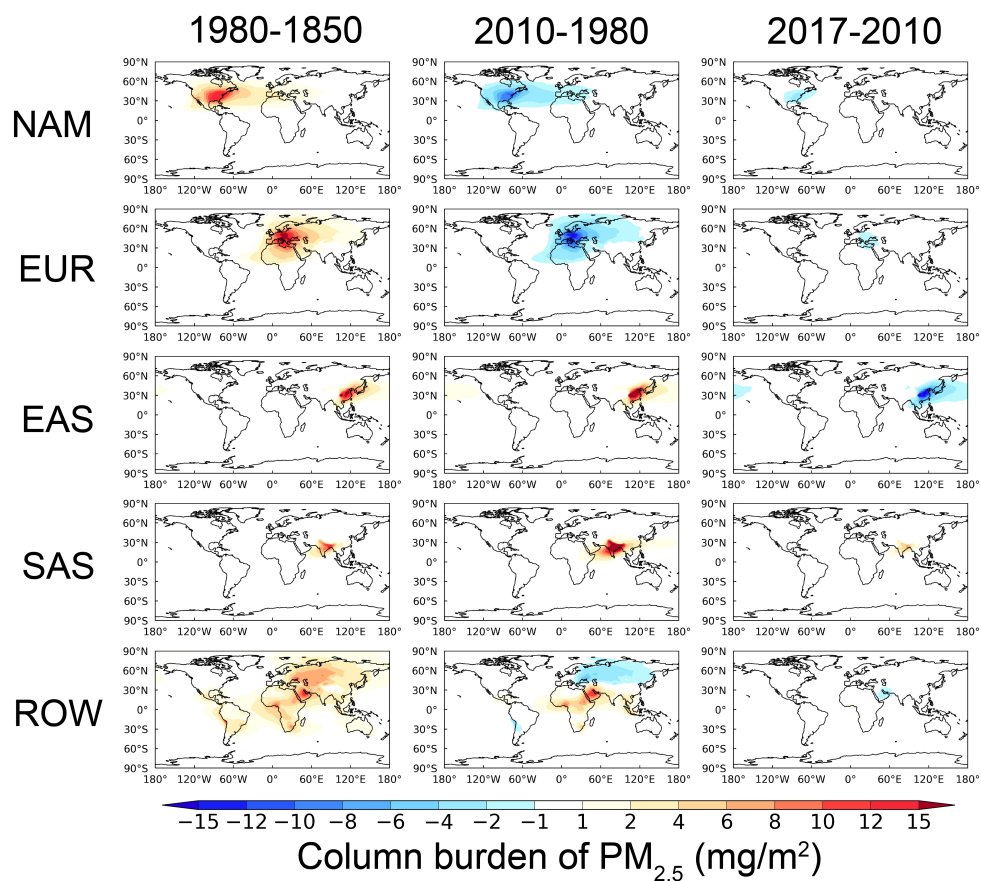
624

625



626

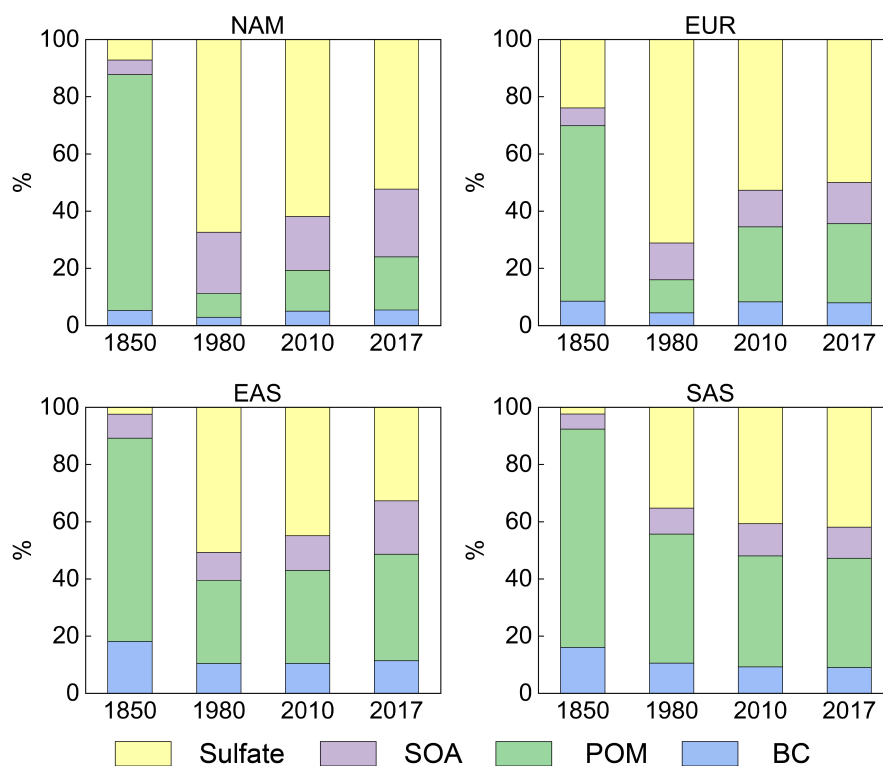
627 **Figure 4.** Changes in near-surface mass concentration (µg/m³) of anthropogenic PM_{2.5}
628 contributed by the 5 tagged source regions (NAM, EUR, EAS, SAS and ROW from top to
629 bottom) between 1850 and 1980 (left), between 1980 and 2010 (middle), and between 2010
630 and 2017 (right).
631



632

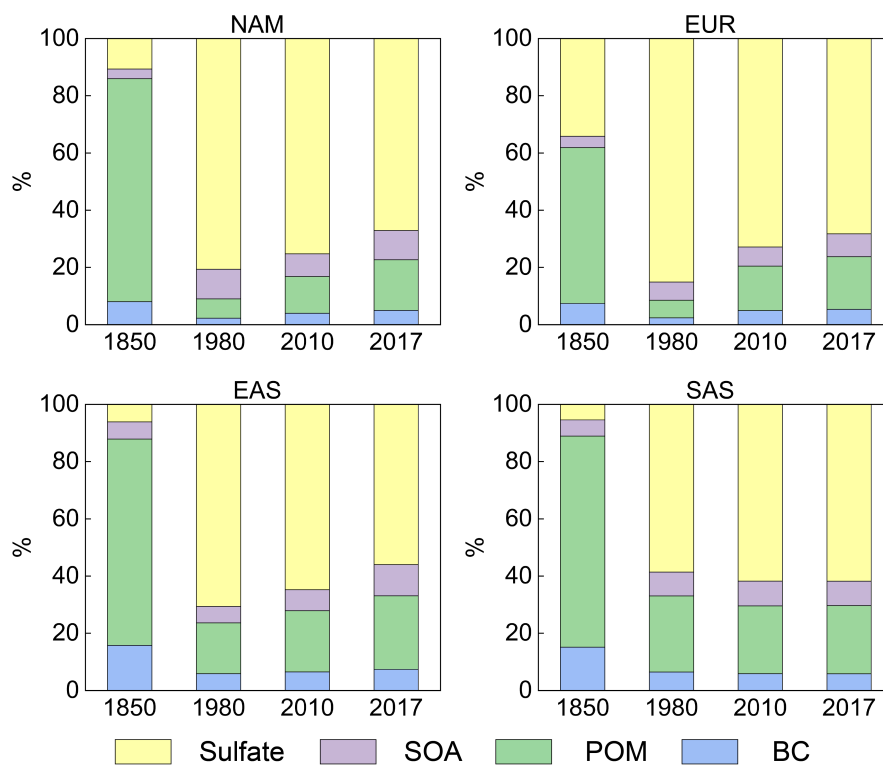
633 **Figure 5.** Same as figure 4 but for column burden (mg/m²) of anthropogenic PM_{2.5}.

634



635

636 **Figure 6.** Percentage contributions (%) of aerosol species including BC, POM, SOA and
637 sulfate to the near-surface mass concentrations of $PM_{2.5}$ averaged over the four major emission
638 source regions (NAM, EUR, EAS and SAS) in the focused four years (1850, 1980, 2010 and
639 2017).
640

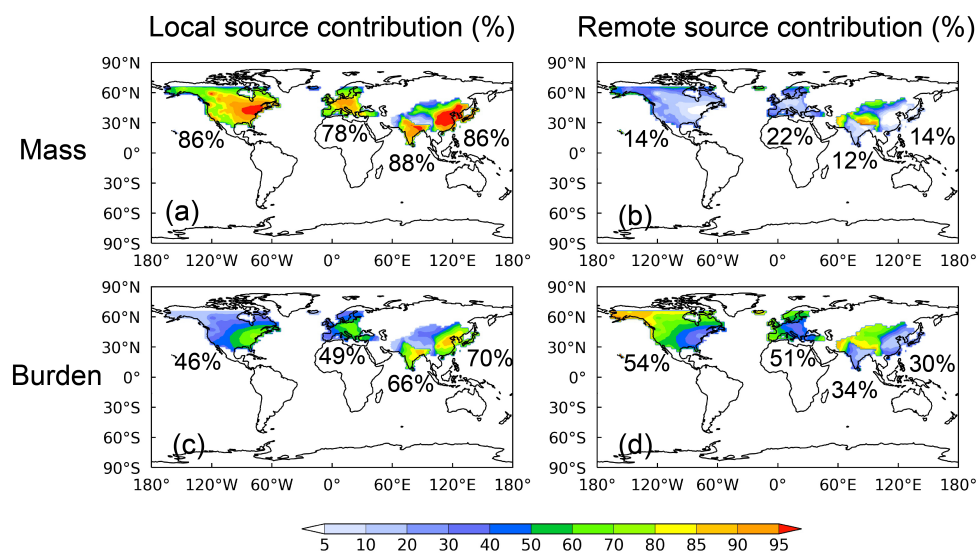


641

642

643

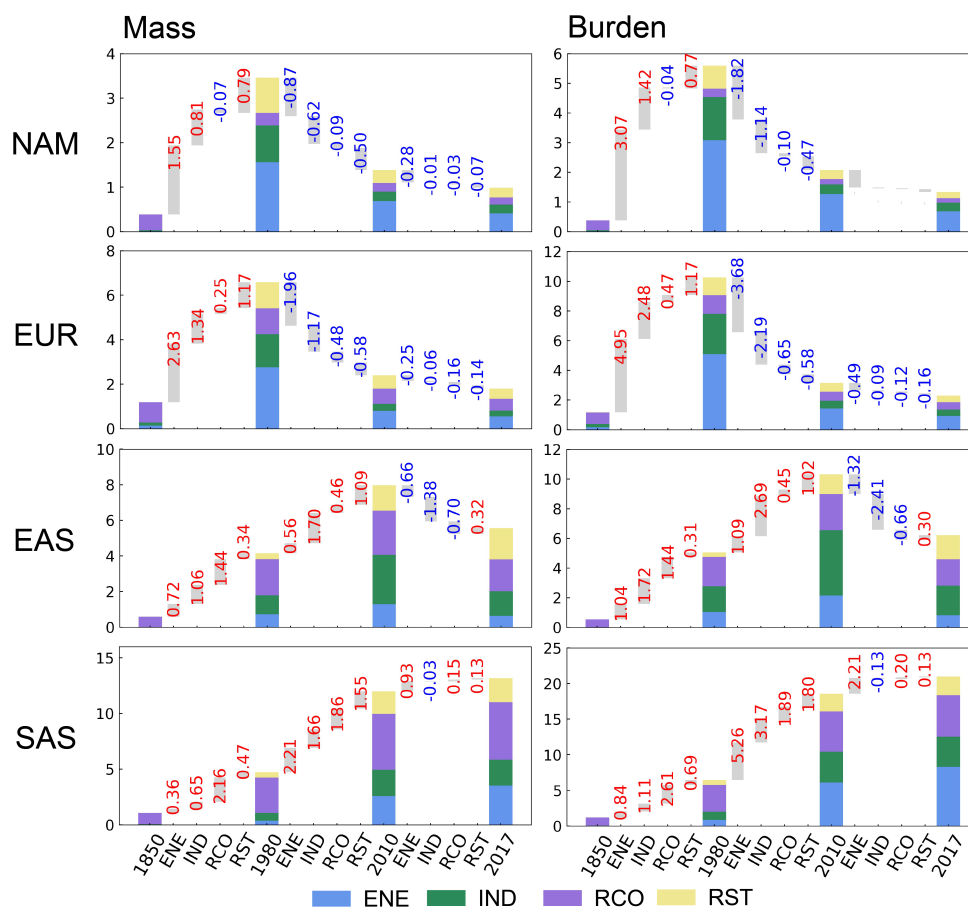
Figure 7. Same as figure 6 but for contributions to regional column burdens.



644

645 **Figure 8.** Relative contributions (%) from (a, c) local and (b, d) remote anthropogenic
646 emissions to the near-surface mass concentrations and column burdens of PM_{2.5} in the four
647 targeted regions (NAM, EUR, EAS and SAS) in 2010. Numbers marked on the figure are the
648 regional average over the four individual targeted regions.

649



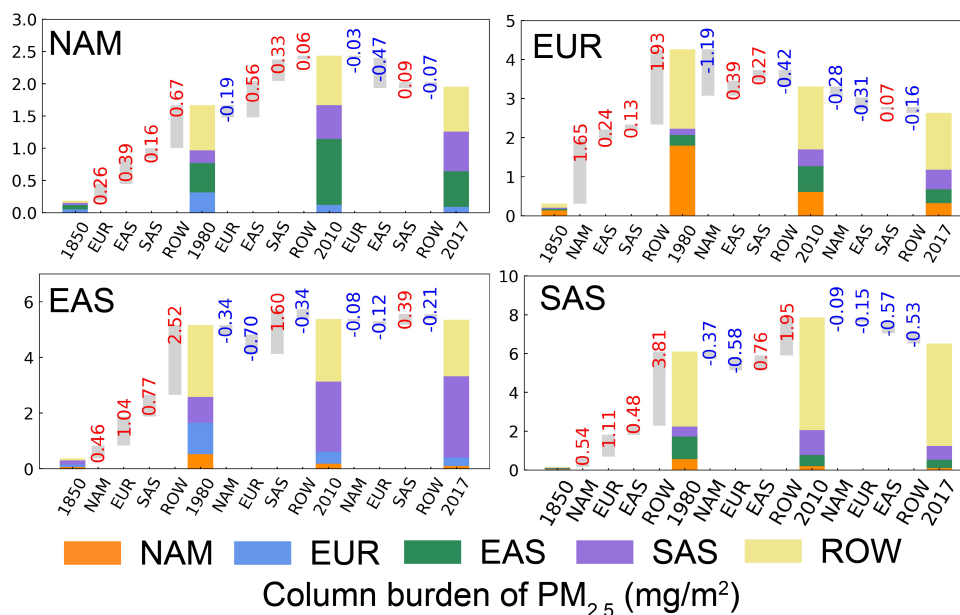
650

651

Figure 9. Local source contributions from four individual emission sectors (ENE, IND, RCO and RST) to the near-surface mass concentrations ($\mu\text{g}/\text{m}^3$, left) and column burdens (mg/m^2 , right) of anthropogenic $\text{PM}_{2.5}$ in the four targeted regions (NAM, EUR, EAS and SAS from top to bottom) for years 1850, 1980, 2010 and 2017 (in color bars). Grey bar and numbers in between two years show the change in sector contributions. Positive values are shown in red and negative values are shown in blue.

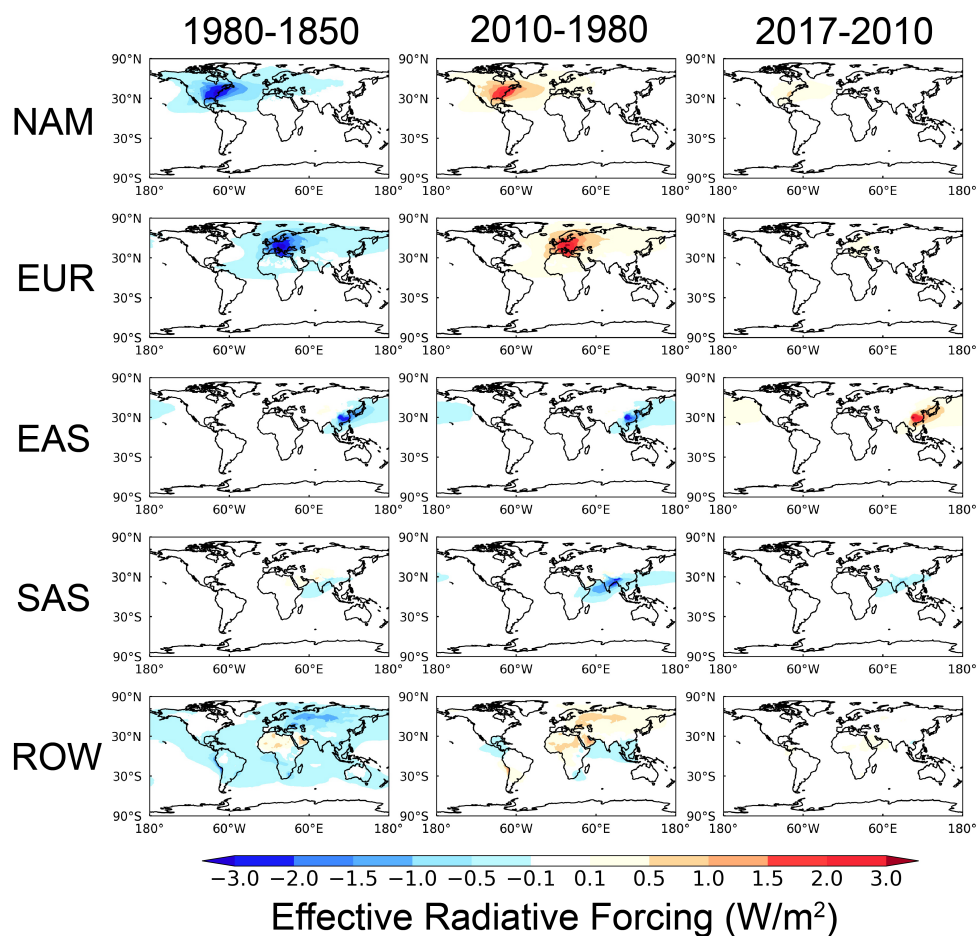
656

657



658

659 **Figure 10.** Same as Figure 9, but for contributions from the remote tagged source regions to
 660 the column burdens (mg/m²) of anthropogenic PM_{2.5} in the four targeted regions (NAM, EUR,
 661 EAS and SAS).
 662



663

664

Figure 11. Changes in effective radiative forcing (W m^{-2}) at the top of the atmosphere due to

665

aerosol-radiation interactions between 1850 and 1980 (left), between 1980 and 2010 (middle),

666

and between 2010 and 2017 (right) attributed to the changes in anthropogenic emissions from

667

NAM, EUR, EAS, SAS and ROW (from top to bottom).